Information Transfer in Spintronics Networks under Worst Case Uncertain Parameter Errors

A. A. Rompokos[1], F. C. Langbein[2] and E. Jonckheere[1]

***Abstract*— A novel quantum landscape optimization with respect to bias field control inputs is developed with the goal of achieving optimal transfer fidelity subject to robustness against bias field, spin couplings and other uncertainties. This objective is achieved by minimization of a convex combination of fidelity error and worst-case perturbation of fidelity error under directional perturbation of uncertain parameters. The novelty is that the end-point perturbations of the parameters are points of a random uniform sampling of the sphere centered at the nominal values of the parameters. This reveals that the previously developed perfect state transfer with zero sensitivity solution keeps high fidelity and robustness under large rather than differential perturbations.**

I. Introduction

Over the past few years, the search of control laws for quantum devices to achieve ultra-accurate tasks under technological limitations on both the devices and the implementation of the control inputs has emerged of paramount importance for the quantum revolution to be successful [1]–[3]. More technically speaking, the hope is to achieve high fidelity simultaneously with high robustness. The fundamental limitations on achievable performance imposed by traditional control under the single degree of freedom configuration appears to place a roadblock to such endeavor [4]. However, the difficulty of implementing a traditional feedback around an uncertain quantum system has led to quantum control architectures differing from the formalized traditional control architecture [5], leaving a glimpse of hope that an ideal high-fidelity, high-robustness solution could be found. In fact, such an elusive control law has been found for single excitation transfer in spin chains [6, Th. 3]: the so-called super-optimal fidelity solution has vanishing fidelity error and vanishing differential sensitivity relative to Hermitian perturbations of the Hamiltonian. This overshadows the adversarial game approach [7], in which the controller is designed under the worst possible circumstances in the uncertainties. However, the game approach is not restricted to differential perturbations and could give the elusive differentially optimal solution of [6] some numerical robustness by considering larger variations than the differential ones.

Specifically, the design optimization criterion is a convex combination of fidelity error and worst-case deviation of the fidelity under uniform sampling of the directions of uncertainties of the parameters. An optimisation over a weighted sum of fidelity error and its first derivatives would yield a "flat" minimum. But here instead of first order derivatives, we use finite differences, which then still seek for a flatter—hence more robust—minimum, depending on the range.

Regarding applications, emphasis is on excitation-encoded information transfer in spin chains.

[1] Dept. of Elec. Eng., Univ. of Southern California, Los Angeles, CA 90089 {jonckhee,rompokos}@usc.edu

[2]School of Computer Science and Informatics, Cardiff University, UK {frank@langbein.org}

II. Theory and Problem Setup

A. Network of Spins & Control Problem

This paper investigates information propagation in networks of N spins. Our focus is a spin-1/2 system, with two spin states, $|0\rangle$ and $|1\rangle$, where the Hamiltonian $\boldsymbol{H}_\Delta$ is given by [8]:

$$\boldsymbol{H}_\Delta = \sum_{n=1}^{N} d_n Z_n + \sum_{n\neq m}^{N} J_{mn}\left(X_n X_m + Y_n Y_m\right). \qquad (1)$$

The first term of the RHS of Eq. (1) is the control part of the Hamiltonian where d_n is the external control input on spin # n. The second term denotes the unforced spin dynamics. X_n is an operator in the 2^N-dimensional Hilbert space and is defined by the tensor product of $N-1$ identity operators and the Pauli operator σ_x in the n^{th} position. Operators Y_n and Z_n are defined in the same way as X_n using the Pauli operators σ_y and σ_z, respectively, and J_{mn} denotes the coupling between the n^{th} and m^{th} spins. We consider a network with chain topology, i.e., there are only couplings between neighboring spins; thus $J_{mn}=0$ for $m\neq n+1$ and we further assume that the spins are linked with the same strength, which is normalized to 1 for simplicity, resulting in $J_{n,n+1}=1$. Based on the above, restricting $\boldsymbol{H}_\Delta$ from Eq. (1) to the single excitation subspace where one and only one spin is excited, we obtain the following Hamiltonian:

$$\boldsymbol{H}_\Delta = \begin{bmatrix} d_1 & 1 & 0 & \dots & \\ 1 & d_2 & 1 & \dots & \\ 0 & & \ddots & & \\ & & & 1 & d_N \end{bmatrix}.$$

H_Δ is a tridiagonal matrix containing the vector of control inputs $\Delta = [d_1 \quad d_2 \dots d_N]$ in the diagonal and the couplings of 1 in the sub- and super-diagonals. The diagonal element d_n represents the bias field or voltage that controls the potential of the n^{th} spin [8].

The dynamics of the information propagation in a chain with a single excited qubit are given by Schröndiger's equation:

$$i\hbar\frac{\partial}{\partial t}\Psi(t) = \boldsymbol{H}_\Delta \Psi(t), \qquad (2)$$

where $\Psi(t)$ is an N-dimensional unit-norm vector denoting the state of the spins. A common performance metric of state propagation is the overlap between a target state $|\mathrm{OUT}\rangle$ and the state propagated by the system's dynamics (Eq. (2)) with initial state $|\mathrm{IN}\rangle$:

$$F_t(\Delta) \triangleq |\langle \mathrm{OUT}| e^{-\mathrm{i}\boldsymbol{H}_\Delta t} |\mathrm{IN}\rangle|^2. \tag{3}$$

Eq. (3) defines the ***fidelity*** $F_t(\Delta)$ and can be interpreted as the probability of successful information propagation; thus $0 \leq F_t(\Delta) \leq 1$. The ***fidelity error*** or infidelity is defined as $1 - F_t(\Delta)$. The time t is the time required to complete the propagation of an excitation in the network. As shown in [8], the parameter t greatly affects the fidelity and it is imperative to treat it as a variable rather than as preselected. Thus, our goal becomes the computation of the appropriate input vector Δ and time t such that the fidelity $F_t(\Delta)$ is maximized:

$$\min_{\Delta,t} \quad (1 - F_t(\Delta)). \tag{4}$$

Relevant work [9] has shown that the landscape of Eq. (4) is complicated with many local maxima/minima, making the accurate solution for the optimal parameters Δ and t a challenging task. In [10], the authors modify convex optimization methods to maximize the fidelity subject to model uncertainties and in [11] Khalid et al. use model-agnostic reinforcement learning methods to explore the complex fidelity surface and obtain high fidelity solutions.

B. Robustness under Uncertainties

In practice, the bias controls d_n applied as inputs to the spin network (theoretically to the Hamiltonian) will involve field uncertainties. Maintaining high fidelity given the input or Hamiltonian uncertainties requires robustness-aware solutions to transfer fidelity optimization. In addition to maximizing $F_t(\Delta)$, we want the solution that yields high fidelity to be robust against such uncertainties as those of the bias fields and the couplings. Thus we modify the optimization problem of Eq. (4) to minimize a convex combination of fidelity error and worst-case large-scale sensitivity:

$$\min_{\Delta,t} \quad \alpha\,(1 - F_t(\Delta)) + (1-\alpha)\|\delta F_t(\Delta)\|_\infty. \tag{5}$$

The first term of Eq. (5) penalizes the fidelity error whereas the second term of (5) penalizes the worst-case perturbation of the fidelity for a uniform sampling of directional variations of the control parameters. δ is the directional variation operator along the unbiased sample of directions, and the infinity-norm indicates the worst-case direction of the variation of $F_t(\Delta)$. By appropriately choosing the parameter α in problem (5), we opt to slightly lower the fidelity to achieve significantly higher robustness.

The new metric $\|\delta F_t(\Delta)\|_\infty$ is a large-scale version of the differential metric,

$$\partial F_t(\Delta) = \max_{\|h\|=1} |\nabla F_t(\Delta) \cdot h|$$

Intuitively, if $\partial F_t(\Delta) = 0$, the peak of the fidelity is "flat" hence giving the design some good sensitivity properties; if on the other hand $\|\delta F_t(\Delta)\|_\infty = 0$ the fidelity "peak" would be "flatter" across a larger region of Δ's, hence with better robustness properties. This resolves the concern that points with high fidelity lie in sharp peaks of the optimization landscape and even minor in scale noise or uncertainties can greatly increase the fidelity error.

As shown in [6] and using the first order optimality criteria, the differential of the fidelity with respect to any control input and the differential with respect to coupling uncertainties are zero. But a better solution would be one that results in high fidelity and low *large-scale* differential. This solution is attempted to be achieved with the parameter $0 \leq \alpha \leq 1$ which is set to balance the tradeoff between fidelity $F_t(\Delta)$ and robustness $\|\delta F_t(\Delta)\|_\infty$.

C. Fidelity Large-Scale Differential

We define the fidelity large-scale differential as the forward difference of the fidelity along Δ or other perturbative directions.

1) Perturbation I: In a network of N spins, the ***fidelity large-scale differential*** δF ***relative to a basis*** $\{e_i\}$ is an N-dimensional vector with i^{th} component given by

$$[\delta F_t^e]_i = \frac{F_t(\Delta + \varepsilon e_i) - F_t(\Delta)}{\varepsilon}, \tag{6}$$

where ε is a larger than infinitesimal change that represents the strength of such change and e_i is the i^{th} standard basis vector.

2) Perturbation II: More generally, the ***fidelity large-scale differential for a sample of vectors*** h ***uniformly distributed over the unit sphere*** is defined as

$$\delta F_t^h = \frac{F_t(\Delta + \varepsilon h) - F_t(\Delta)}{\varepsilon}, \tag{7}$$

where ε is the strength.

3) Hamiltonian perturbation: We also consider uncertainties in J-couplings between the spins in the Hamiltonian. Those uncertainties can be caused by coupling identification errors, by non-homogeneous bias fields, or chain engineering errors. The perturbed Hamiltonian is then given by

$$\boldsymbol{H}_\Delta^p = \sum_{n=1}^{N} d_n Z_n + \sum_{n\neq m}^{N} J_{mn}(1+\varepsilon_n)\,(X_n X_m + Y_n Y_m)\,. \tag{8}$$

Here, contrary to the e_i and h cases, ε is a 0-mean random noise of standard deviation σ_ε : $\varepsilon_n \sim N(0, \sigma_\varepsilon)$. Using the perturbed Hamiltonian, we compute the corresponding fidelity

$$F_t^p(\Delta) \triangleq |\langle \mathrm{OUT}| e^{-\mathrm{i}\boldsymbol{H}_\Delta^p t} |\mathrm{IN}\rangle|^2$$

and define the ***fidelity large-scale differential corresponding to Hamiltonian perturbation*** $\boldsymbol{H}_\Delta^p$:

$$\delta F_t^p = \frac{F_t^p(\Delta) - F_t(\Delta)}{\sigma_\varepsilon}. \tag{9}$$

The dimension of the vector δF_t^p is the size of the random sampling of ε.

4) Computational complexity: Each component of either δF_t^e, δF_t^h or δF_t^p requires evaluation of a matrix exponential, which for every single directional perturbation requires $O(N^3)$ flops (assuming diagonalization or Pade approximation is used).

III. Results & Discussion

A. Solution Perturbations I

Initially we examine the fidelity and robustness performance of our formulation of Eq. (5) using the robustness metric given by Eq. (6). For that matter, we investigate the effect of the parameter α in weighing the infidelity $1-F_t(\Delta)$ and robustness $\delta F_t^e(\Delta)$. We ran simulations with increasing α. For each α we repeated the simulation 10 times, each time for different N ($4 \leq N \leq 12$), $|\text{IN}\rangle$ and $|\text{OUT}\rangle$ randomly chosen. The average performance of the 10 trials for each α for strength level $\varepsilon = 5\%$ is presented in Fig. 1. We observe that increasing α results in lower infidelity and worse robustness since the large-scale differential is significantly increased. It should be mentioned, however, that for some α we obtain good performance on average for both fidelity error and large-scale sensitivity, the point $(0.025, 0.25)$ that lies at the bottom left-hand corner of the plot. Such data point contradicts the traditional conflict between error minimization and error sensitivity minimization [4].

Finally we compare the effect of α in each individual metric. Using the same simulation setup as above, we present the distributions of $1-F_t(\Delta)$ and $\delta F_t^e(\Delta)$ in Figs. 2 and 3, resp. As expected, for small α, the infidelity distribution spans the whole range of $[0, 1]$, while the large-scale differential remains low. Increasing α results in an increasing trend in the differential and a decreasing one in the infidelity. Thus, statistically, a Pareto-like conflict between two objectives develops where improving one objective is accompanied by a deterioration of the other objective.

B. Solution Perturbations II

In this section we further investigate the robustness performance of Eq. (5) under control input uncertainties in any direction, as per Eq. (7). We designed a similar experimental setup as in Sec. III-A and simulated Eq. (5) for 20 randomly chosen N, $|\text{IN}\rangle$ and $|\text{OUT}\rangle$. The results are presented in Figs. 4-6.

In Figs. 5 and 6, we note that α has similar effect as in the results of Sec. III-A. Namely, increasing α decreases the fidelity error and increases the large-scale sensitivity. In this case, we can also achieve a result in which both the infidelity $1-F_t(\Delta)$ and worst-case differential $\delta F_t^h(\Delta)$ are kept low, the $(0.03, 0.24)$ data point in the bottom left-hand corner of Fig. 4.

C. Hamiltonian Perturbations

In this section we consider the uncertainties in the Hamiltonian $\boldsymbol{H}_\Delta^p$ rather than in the control input Δ, as defined by Eq. (9). We simulated Eq. (5) using δF_t^p as robustness metric, for different α and σ_ϵ. The number of spins N was randomly chosen between 4 and 12, and $|\text{IN}\rangle$ and $|\text{OUT}\rangle$ were randomly sampled from $\{1, \ldots, N\}$.

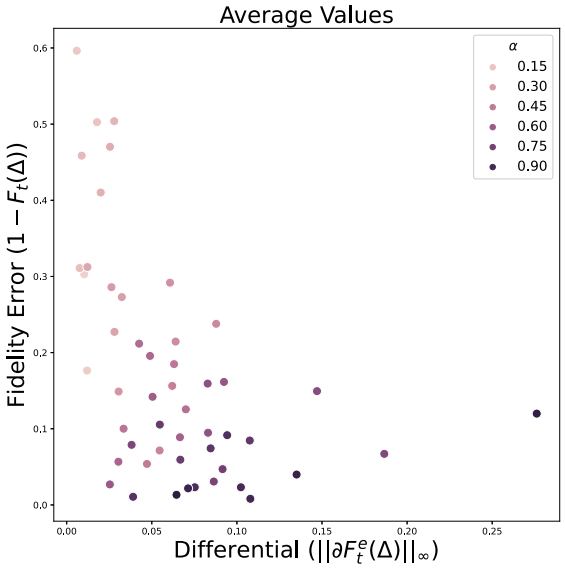

Fig. 1. Scatter plot of average fidelity error $1 - F_t(\Delta)$ vs $\|\delta F_t^e(\Delta)\|_\infty$ for bias field perturbations. The strength level was set to $\varepsilon = 5\%$ and the range of α was from 0.1 to 1. Each simulation of Eq. (5) was ran 10 times for the same α value and the average results per α are presented.

Fig. 7 shows the effect of the parameter α on fidelity error and robustness. For each α we simulated Eq. (5) 20 times, and each time we sampled H_Δ^p 10 times. Each point in the plot represents the average fidelity error and large-scale differential for a specific α. Overall, the fidelity error is relatively low ranging from 1% to 10% while the differential shows greater variance. The same figure illustrates the tradeoff between minimizing the two conflicting objectives,

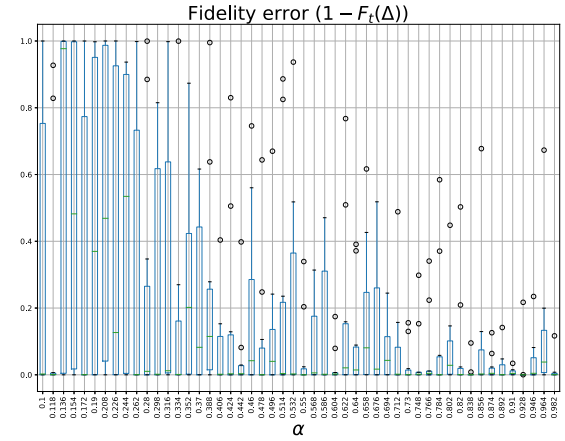

Fig. 2. Infidelity $1 - F_t(\Delta)$ distributions for bias field perturbations. The strength level was set to $\varepsilon = 5\%$ and the range of α was from 0.1 to 1. Each simulation of Eq. (5) was ran 10 times for the same α value.

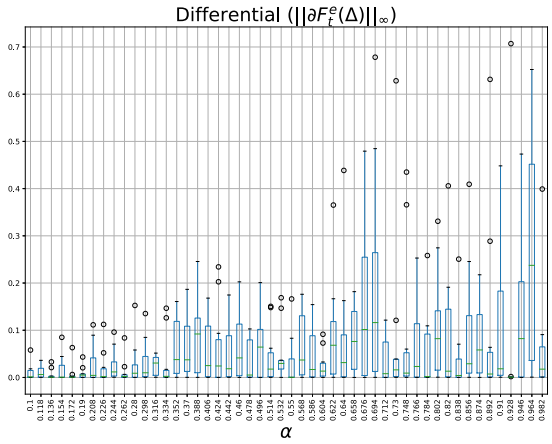

Fig. 3. Worst-case differential $\|\delta F_t^e(\Delta)\|_\infty$ distribution for bias field uncertainties. The strength level was set to $\varepsilon = 5\%$ and the range of α was from 0.1 to 1. Each simulation of Eq. (5) was ran 10 times for the same α value.

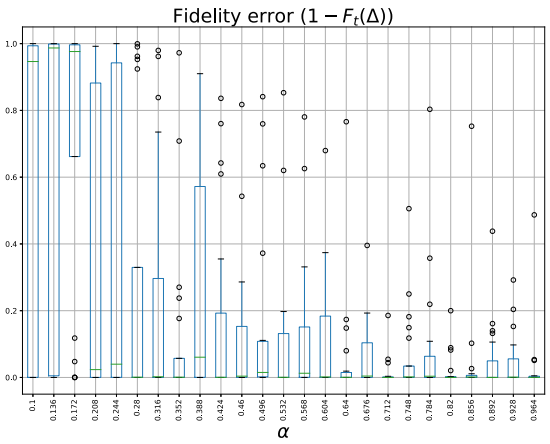

Fig. 5. Infidelity $1 - F_t(\Delta)$ for bias field uncertainties. The strength level was set to $\varepsilon = 5\%$ and the range of α was from 0.1 to 1. Each simulation of Eq. (5) was ran 20 times for the same α value.

i.e. fidelity error and differential: low α values yields low $\|\delta F_t(\Delta)\|_\infty$ hence increased robustness performance, at the cost of higher fidelity error. As for the case of bias field uncertainties, the case of Hamiltonian uncertainties also reveals a near perfect solution, but this time in the sense of a *Pareto-optimal* point $(0.1, 0.01)$ at the bottom left-hand corner of Fig. 7.

From Figs. 8 and 9, as we increase α, the infidelity is slightly decreased while $\|\delta F_t(\Delta)\|_\infty$ is slightly increased.

Finally, the direct comparison of the fidelity optimization (Eq. (4)) and mixed sensitivity optimization (Eq. (5)) reveals that mixed sensitivity offers increased robustness performance. For the same N, $|\text{IN}\rangle$ and $|\text{OUT}\rangle$ we simulated Eq. (4) and Eq. (5) for varying σ_ϵ. The distribution of the robustness $\delta F_t^p(\Delta)$ for 20 simulation runs for each noise level σ_ϵ is presented in Fig. 10, where δF_t^p is lower for mixed sensitivity at each noise level. For the same experimental setup, we also present the infidelity in Fig. 11. For every noise level ϵ, the fidelity error is greater for the mixed sensitivity, a fact that indicates the trade-off between fidelity and robustness.

IV. Conclusion

Classical control places some severe limitations on designs of the single degree of freedom configuration attempting to

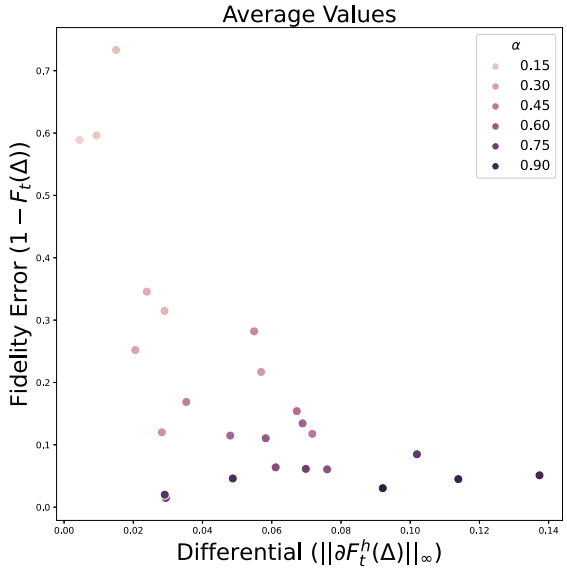

Fig. 4. Scatter plot of average infidelity $1 - F_t(\Delta)$ vs $\|\delta F_t^h(\Delta)\|_\infty$ for input uncertainties. The strength level was set to $\varepsilon = 5\%$ and the range of α was from 0.1 to 1. Each simulation of Eq. (5) was ran 10 times for the same α value and the average results per α are presented.

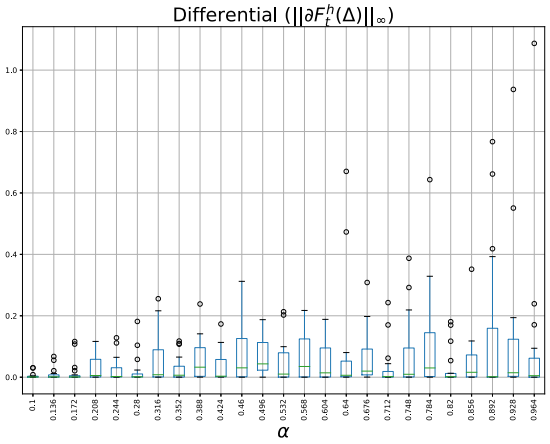

Fig. 6. Worst-case differential $\|\delta F_t^h(\Delta)\|_\infty$ distribution for bias field perturbations. The strength level was set to $\varepsilon = 5\%$ and the range of α was from 0.1 to 1. Each simulation of Eq. (5) was ran 20 times for the same α value.

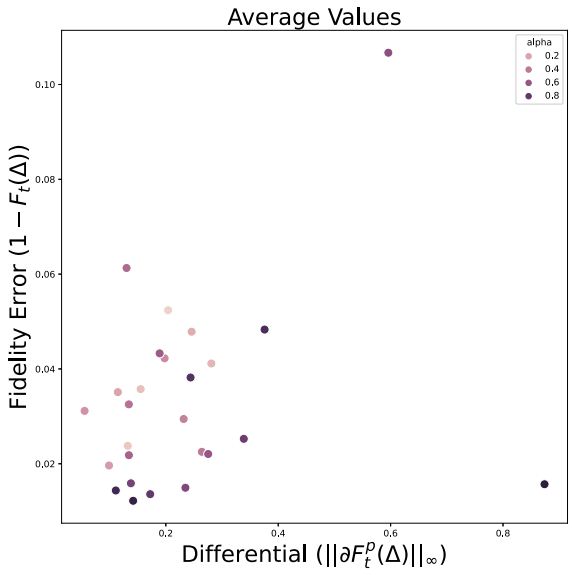

Fig. 7. Scatter plot of average infidelity $1 - F_t(\Delta)$ vs $\|\delta F_t^p(\Delta)\|_\infty$ for Hamiltonian perturbations. The noise level was set to $\varepsilon = 5\%$ and the range of α was from 0.01 to 0.999 with step 0.04. Each simulation of Eq. (5) was ran 20 times for the same α value and the average results per α are presented.

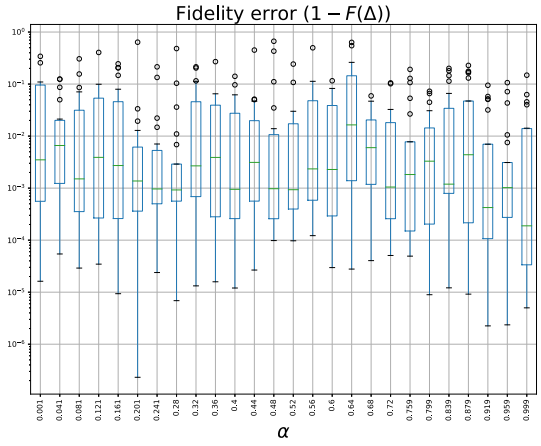

Fig. 8. Fidelity error $1-F_t^p(\Delta)$ distributions for Hamiltonian perturbations for different α. The noise level was set to $\varepsilon = 5\%$ and the range of α was from 0.01 to 0.999 with step 0.04. Each boxplot contains 20 samples from simulations of Eq. (5). Despite the perturbations, our approach kept the fidelity error in relative low levels ($< 10\%$), even though in some cases we have some outlier values.

achieve small error and small sensitivity of error to perturbation [4]; however, the 2-degree of freedom configuration alleviates such limitations [12]. Architecturally, information transfer by bias field control appears to be of *some* 2-degree of freedom configuration with an additional global phase along the loop [5]. This at least partially explains—from a classical control perspective—earlier studies [6], [13] pointing to concordance between small error and small *differential* sensitivity to perturbations. The scatter plots of Figs. 1, 4, and 7 show the extent to which such concordance holds for *large* perturbations. The case of Hamiltonian perturbation of Fig. 7 with the data points clustering to the left appears to defy this conflict, whereas the case of sphere sampling of Fig. 4 with its hyperbolic cluster is more mitigated. However, for all 3 cases, there is an α (close to 0.9) achieving concordance between error and large-scale sensitivity. Such conclusion corroborates the earlier findings of [6], [13] by showing that they hold under variation larger than the differential one—in a move that parallels the development of classical robust control when it transitioned from differential to large variations [4].

APPENDIX

A. Uniform sampling of the sphere

Eq. (7) explores different directions defined by the unit vector h. Since $h \in \mathbb{R}^N$ and $\|h\| = 1$, h runs on the unit sphere $\mathbb{S}^{N-1}$. Clearly, uniform sampling of the sphere is required to have an accurate estimate of the variation along the worst direction with a minimum number of function calls. Such sampling can also be defined as *fair,* that is, it does not privilege any direction. Formally, a ***uniform sampling of the sphere*** is a set of points that is invariant under discrete groups of rotations around N basis axis. For example, the vertices of a regular icosahedron form a 12-point uniform sampling of the sphere invariant under $2\pi/5$ rotation about the axis from the center of the sphere to the vertex. Symmetry about axes from the center of the sphere to the centers of the faces involves a representation $A_5 \to \mathrm{SO}(\mathbb{R}^3)$ of the alternating group on 5 elements. The problem is that construction of a uniform sampling by forcing rotational invariant is not an easy task. Therefore, in the sequel, we will construct a fair random sampling by a random draw of a N-dimensional

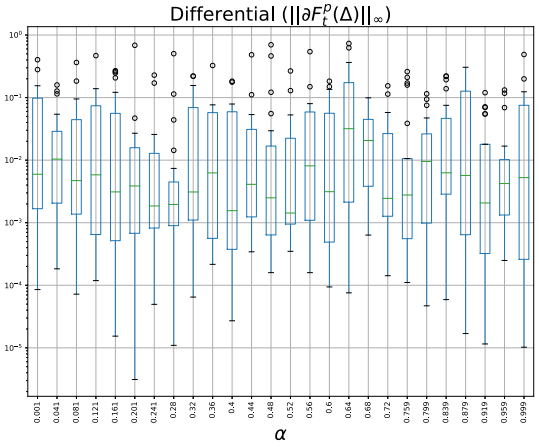

Fig. 9. Worst-case differential $\|\delta F_t^p(\Delta)\|_\infty$ distributions for Hamiltonian perturbations for different α. The noise level was set to $\varepsilon = 5\%$ and the range of α was from 0.01 to 0.999 with step 0.04. Each boxplot contains 20 samples from simulations of Eq. (5). Despite the perturbations, our approach kept the fidelity error in relative low levels ($< 10\%$), even though in some cases we have some outlier values.

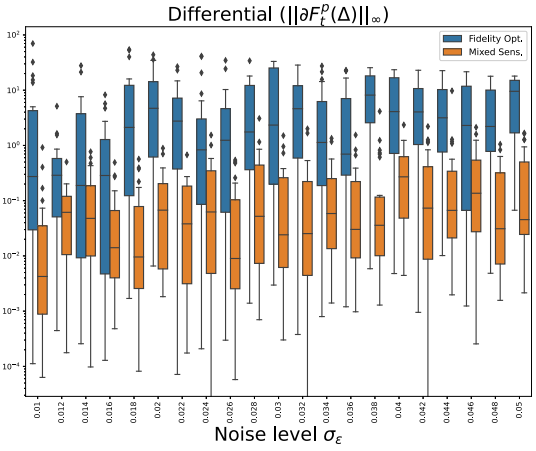

Fig. 10. Robustness performance $\|\delta F_t^p(\Delta)\|_\infty$ distributions for Hamiltonian perturbations of different noise level ϵ. Each boxplot contains samples from simulations of Eqs. (4) and (5) for $0.01 \leq \alpha \leq 0.999$. Penalizing the differential and the infidelity clearly increases the robustness performance of the input. For each noise level σ_ε, mixed sensitivity yields lower differential δF_t^p. Note the logarithmic scale of the y-axis.

zero-mean Gauss distribution after normalizing the sample vectors [14].

References

[1] M. Christandl, N. Datta, *et al.*, "Perfect transfer of arbitrary states in quantum spin networks," *Phys. Rev. A*, vol. 71, p. 032 312, 3 Mar. 2005.

[2] E. Jonckheere, F. C. Langbein, and S. G. Schirmer, "Information transfer fidelity in spin networks and ring-based quantum routers," *Quantum Information Processing*, vol. 14, no. 12, pp. 4751–4785, Dec. 2015.

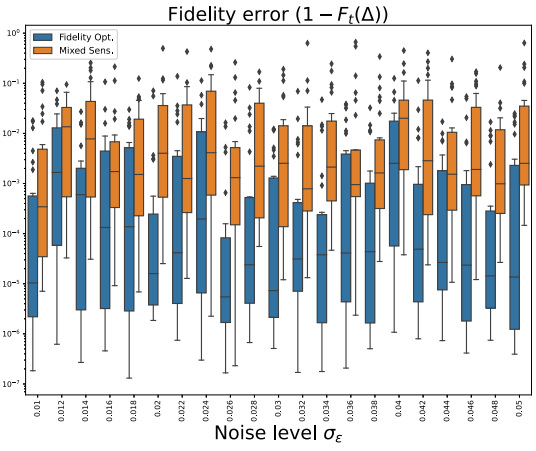

Fig. 11. Comparison of the distributions of the fidelity error $1 - F_t(\Delta)$ using fidelity optimization of Eq. (4) and mixed sensitivity as described by Eq. (5) for $0.01 \leq \alpha \leq 0.999$. Minimizing only the fidelity error, yields near optimal information transfer ($> 97\%$). As expected, penalizing both the infidelity and the differential increases the fidelity error, which is still maintained in low levels ($\leq 15\%$). The y-axis is in logarithmic scale.

[3] J. Majer, J. Chow, *et al.*, "Coupling superconducting qubits via a cavity bus," *Nature*, vol. 449, no. 7161, pp. 443–447, Sep. 2007, ISSN: 1476-4687.

[4] M. G. Safonov, A. J. Laub, and G. L. Hartmann, "Feedback properties of multivariable systems: The role and use of the return difference matrix," *IEEE TAC*, vol. AC-26, no. 1, pp. 47–65, Feb. 1981.

[5] E. Jonckheere, S. Schirmer, and F. Langbein, "Effect of quantum mechanical global phase factor on error versus sensitivity limitation in quantum routing," in *58th IEEE CDC*, Dec. 2019, pp. 1139–1344.

[6] S. G. Schirmer, E. A. Jonckheere, and F. C. Langbein, "Design of feedback control laws for information transfer in spintronics networks," *IEEE TAC*, vol. 63, no. 8, pp. 2523–2536, Aug. 2018.

[7] X. Ge, H. Ding, *et al.*, "Robust quantum control in games: An adversarial learning approach," *Phys. Rev. A*, vol. 101, p. 052 317, 5 May 2020.

[8] F. C. Langbein, S. Schirmer, and E. Jonckheere, "Time optimal information transfer in spintronics networks," in *54th IEEE CDC*, 2015, pp. 6454–6459.

[9] M. Y. Niu, S. Lu, and I. L. Chuang, "Optimizing qaoa: Success probability and runtime dependence on circuit depth," *arXiv: Quantum Physics*, 2019.

[10] Y. Dong, X. Meng, *et al.*, "Robust control optimization for quantum approximate optimization algorithms," in *21st IFAC World Congress*, 2020, pp. 242–249.

[11] I. Khalid, C. A. Weidner, *et al.*, "Reinforcement learning vs. gradient-based optimisation for robust energy landscape control of spin-1/2 quantum networks," in *60th IEEE CDC*, 2021, pp. 4133–4139.

[12] Y. Xie and A. Alleyne, "Robust two degree-of-freedom control of MIMO system with both model and signal uncertainties," in *19th IFAC World Congress*, Aug. 2014, pp. 9313–9320.

[13] E. Jonckheere, S. Schirmer, and F. Langbein, "Jonckheere-Terpstra test for nonclassical error versus log-sensitivity relationship of quantum spin network controllers," *Int. J. of Robust and Nonlinear Control*, vol. 28, no. 6, pp. 2383–2403, Apr. 2018.

[14] M. E. Muller, "A note on a method for generating points uniformly on n-dimensional spheres," *Commun. ACM*, vol. 2, pp. 19–20, 1959.